

Scattering description of edge states in Aharonov-Bohm triangle chains


Zhi-Hai Liu^{1,*}, O. Entin-Wohlman^{2,†}, A. Aharony², J. Q. You³, and H. Q. Xu^{4,1}

¹*Beijing Academy of Quantum Information Sciences, Beijing 100193, China*

²*School of Physics and Astronomy, Tel Aviv University, Tel Aviv 6997801, Israel*

³*School of Physics, Zhejiang University, Hangzhou 310027, China*

⁴*Beijing Key Laboratory of Quantum Devices, Key Laboratory for the Physics and Chemistry of Nanodevices, and School of Electronics, Peking University, Beijing 100871, China*

 (Received 9 November 2023; revised 14 January 2024; accepted 6 February 2024; published 27 February 2024)

Scattering theory has been suggested as a convenient method to identify topological phases of matter, in particular of disordered systems for which the Bloch band-theory approach is inapplicable. Here we examine this idea, employing as a benchmark a one-dimensional triangle chain whose versatility yields a system that “flows” in parameter space among several members of the topology classification scheme. Our results show that the reflection amplitudes (from both ends of long chains) indicate the appearance of edge states in all (topological and nontopological) cases. For the topological cases, the transmission has a peak at the topological phase transition, located at the Fermi energy. A peak still exists as one moves into the nontopological regions, where another transmission peak may occur at nonzero energy, at which an edge state appears in the isolated chain. For finite chains, the transmission peak depends strongly on their coupling with the leads, and not on the phase transition of the isolated chain. In any case, the appearance of a transmission peak is insufficient to conclude that the system undergoes a topological phase transition.

DOI: [10.1103/PhysRevB.109.L081408](https://doi.org/10.1103/PhysRevB.109.L081408)

Introduction. Building on the bulk-boundary correspondence, topological phases of matter are characterized by the emergence of edge or surface states at the Fermi energy [1–3], between the system and the vacuum. Bound states in a finite system affect its scattering properties, suggesting [4] the use of the scattering amplitudes to detect topological phases. This possibility was demonstrated by Fulga *et al.*, who showed that the reflection matrix of a semiinfinite low-dimensional wire obeying a highly symmetric Hamiltonian reflects its topological quantum invariant [4,5]. Scattering theory, as opposed to the Bloch band-structure formalism, operates in real space and thus is particularly suitable for studying topological properties of disordered or inhomogeneous systems [6], inaccessible in the band-structure picture [3]. Conversely, it necessarily connects a finite system to its (nontopological) surroundings [7]. We aim to examine the effectiveness of this method for predicting and detecting topological features.

In the elastic scattering-matrix formalism, the system, e.g., a finite one-dimensional wire, is attached on both sides to two semiinfinite leads, usually described by tight-binding chains. The scattering matrix of such a structure depends naturally on the parameters of these leads, which fix the scattering energy, and on their coupling with the system. These points were largely avoided in previous studies, primarily because they set the scattering energy at the Fermi level [4], adopted an approximate model-independent form of the scattering matrix [8], and focused on the reflection amplitude of a semiinfinite system. Another complication arises from the dependence of the

scattering amplitudes on the wire’s length. For instance, due to the finite-size effect, the threshold for the emergence of nontrivial edge states in a finite Su-Schrieffer-Heeger (SSH) chain [7,9] deviates from the criterion for a topological phase-transition [10,11]. The influence of this ubiquitous size effect on topological features and the scattering amplitudes has not yet attracted much attention, though the scattering formalism seems to be the best tool for exploring the topology of disordered systems.

In addition to the topologically nontrivial symmetry classes [12,13], it has been found recently that systems lacking quantized topological invariants, thus belonging to topologically trivial symmetry classes, may exhibit intriguing phenomena. For instance, unexpected bound states observed experimentally in photonic lattices [14], Rydberg-atom of synthetic dimensions (i.e., engineered degrees of freedom) [15], atomic Aharonov-Bohm (AB) cages [16–19], or proposals for topology in laser systems [20]. However, whether the scattering approach is capable of analyzing the fate of the edge states, as a low-dimensional system moves in parameter space away from topologically nontrivial symmetry classes to topologically trivial ones, is an open question. Sorting out these points is the scope of this paper.

As a benchmark, we study a one-dimensional chain whose versatility yields a scattering matrix that “flows” in parameter space among several members of the topology classification scheme [12,13], including the “BDI” class, which contains the SSH model [7,11,21–24].

As expected, the finiteness of the chain, combined with details of its coupling with the semiinfinite leads, affects the scattering amplitudes and thus may hinder their use as indicators of topological properties characterizing the isolated

*liuzh@baqis.ac.cn

†orawohlman@gmail.com

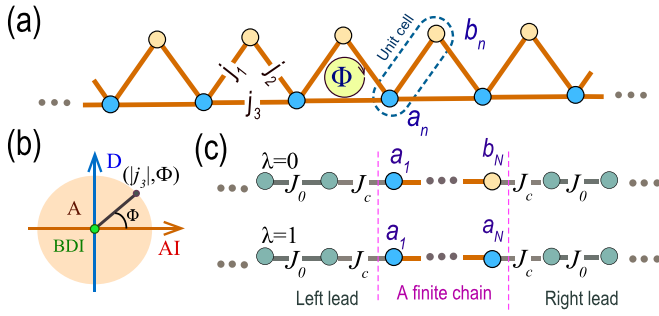


FIG. 1. (a) A triangle chain, hosting two sites a and b in the unit cell, with $j_{1,2}$ and j_3 being the in-cell and out-of-cell tunneling amplitudes. Each triangle is threaded by an Aharonov-Bohm flux Φ in units of the flux quantum. (b) The possible symmetry classes of the triangle chain in the $(|j_3|, \Phi)$ plane, with the “BDI” class at the origin, the “AI” (“D”) class on the horizontal (vertical) axis, and the “A” class occupying the entire plane (except the axes). (c) Two possible configurations of coupling a finite chain of N cells to two semiinfinite leads: in both configurations, the left lead is coupled to an a_1 site, $\lambda = 0$ (1) describe coupling the right lead to a b_N (a_N) site. The tunneling amplitudes on the leads are J_0 , and J_c is the coupling amplitude.

chain. For instance, focusing on the reflection amplitude at the Fermi energy of a topological chain [4,5], one finds that though the size effect may be removed by making the chain semiinfinite (coupling it to a single lead), the phase of the reflection amplitude does depend on the endpoint where it is monitored. Interestingly, we find that the reflection amplitude of a semi-infinite chain belonging to a topologically trivial class can attain the “nontrivial” value -1 , not at the Fermi energy, and an edge state appears on one side of a long isolated chain at that energy, which can be robust against disorder.

Our results show that the reflection amplitudes do indicate the appearance of edge states in all (topological and nontopological) cases. For the topological cases, the transmission has a peak at the topological phase transition (TPT), which happens at the Fermi energy $E = 0$, even in finite long chains. This peak decays as the chain moves into the nontopological regions, where a transmission peak may also occur at nonzero energy. In any case, the appearance of a peak in the transmission is insufficient to conclude a possible TPT. Note that a standard scattering experiment measures the reflection $|r|^2$, not its amplitude r . However, even if the sign of r could be measured, it does not identify the topological phase.

The chain. The model we analyzed [Fig. 1(a)] is built of identical triangles, each penetrated by an AB flux Φ . The vertices are two sites, a and b , connected by staggered tunneling amplitudes, j_1 and j_2 , with nearest-neighbor a sites coupled by j_3 . It is described by

$$\mathcal{H}_\Delta = - \sum_n (j_1 a_n^\dagger e^{i\phi_1} b_n + j_2 b_n^\dagger e^{i\phi_2} a_{n+1} + j_3 a_n^\dagger e^{i\phi_3} a_{n+1} + \text{H.c.}), \quad (1)$$

where a_n^\dagger (b_n^\dagger) creates a spinless electron residing on the a (b) site of the n th cell and $\phi_{i=1,2,3}$ are the partial AB fluxes (in units of $\Phi_0 = h/e$), accumulated on each bond, with $\Phi = \phi_1 + \phi_2 - \phi_3$. Contingent on the values of j_3 and Φ , this chain

“flows” among four symmetry classes. For $j_3 = 0$ the AB flux is irrelevant and the chain becomes the SSH wire [11], whose Hamiltonian obeys time-reversal, particle-hole (PH), and chiral symmetries and thus belongs to the “BDI” class. For a nonzero j_3 and $\Phi = \pm\pi/2$, the Hamiltonian is PH symmetric (details in Ref. [25]), placing the chain in the “D” class. The topology of the high-symmetry classes “BDI” and “D” can be quantified by the Zak phase ϑ_{zak} [25,29], equal to π in the nontrivial topological phase where $|j_1/j_2| < 1$ and zero otherwise. For other parameters the system belongs to the topologically trivial low-symmetry classes “A” and “AI”, see Fig. 1(b), for which ϑ_{zak} is not quantized [25].

Scattering matrix. The scattering formalism requires attaching semiinfinite leads on both sides of a finite chain. Modeling those by identical one-dimensional tight-binding Hamiltonians (with zero on-site energies and tunneling amplitudes J_0), and denoting both tunnel couplings with the chain by J_c , yields two possible edge configurations, see Fig. 1(c); in the $\lambda = 0$ configuration the chain comprises an integer number N of unit cells, for $\lambda = 1$ it does not, the rightmost site being a_N .

The scattering matrix \mathcal{S} relates the amplitudes of the incoming plane waves from the left (right), $A_{L(R)}$, with those of the outgoing waves, $B_{L(R)}$, whose energy E is related to the (dimensionless) wave vector κ ,

$$\begin{bmatrix} B_L \\ B_R \end{bmatrix} = \mathcal{S}_\lambda \begin{bmatrix} A_L \\ A_R \end{bmatrix}, \quad E = -2J_0 \cos(\kappa). \quad (2)$$

Denoted by $\Psi_{a/b}(n)$, ($n = 1, 2, \dots, N$), the wave functions at the a/b sites of the n th cell, continuity at the endpoints implies

$$\frac{J_c}{J_0} \begin{bmatrix} \Psi_a(1) \\ \Psi_\chi(N) \end{bmatrix} = e^{i\kappa} \begin{bmatrix} A_L \\ A_R \end{bmatrix} + e^{-i\kappa} \begin{bmatrix} B_L \\ B_R \end{bmatrix}, \quad (3)$$

where $\chi = b(a)$ for the $\lambda = 0(1)$ configuration. Another relation connecting the endpoints is obtained by the transfer matrix, \mathcal{T} . Let $\mathbf{V}_n = \{\Psi_b(n), \Psi_a(n)\}^T$ be a vector comprising the eigenfunctions of \mathcal{H}_Δ at the two sites of the unit cell, with $1 \leq n \leq N - 2$. The transfer matrix connecting two nearest-neighbor vectors reads

$$\mathbf{V}_{n+1} = \mathcal{T}(E)\mathbf{V}_n. \quad (4)$$

Expressed in terms of a vector $\hat{\mathbf{v}}$,

$$\mathcal{T}(E) = \exp(\alpha \hat{\mathbf{v}} \cdot \boldsymbol{\sigma} - i\zeta),$$

$$\hat{\mathbf{v}} = \frac{e^{i(\phi_1+\beta)}}{2j_2 \sinh(\alpha)} \{w_1 - E, i(w_1 + E), w_2 + e^{-i\phi_1} j_1\},$$

$$\cosh(\alpha) = (E^2 - j_1^2 - j_2^2)/(2|W|) \quad (5)$$

($\boldsymbol{\sigma}$ is the vector of the Pauli matrices). Here $W = j_1 j_2 - E j_3 e^{-i\Phi}$, $\beta = \arg[W]$, $\zeta = \Phi + \phi_3 + \beta$, $w_1 = e^{-2i\phi_1} [E j_1 j_2 - j_3 (j_1^2 e^{-i\Phi} + j_2^2 e^{i\Phi})]/W$, and $w_2 = e^{-i\phi_1} (2j_2 e^{-i\beta} \cosh \alpha + j_1)$.

As usual, the Bloch spectrum of a chain obeying periodic boundary conditions is given by $\mathcal{T}^N \mathbf{V}_n = \mathbf{V}_n$. In that case, α is purely imaginary for a bulk state, while when E is located in the band gap $\exp[\alpha(E)] < -1$ is real [25]. In an open chain, where translational symmetry is broken around the chain-lead junctions, \mathbf{V}_{N-1} and \mathbf{V}_N depend on the specific endpoints

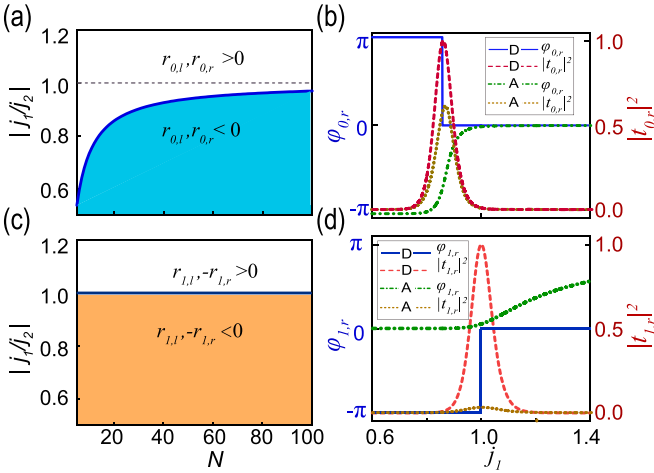


FIG. 2. (a) The sign distribution of the two-sided reflection amplitudes off a finite chain in the $\lambda = 0$ configuration, with the (blue) thick curve being the threshold for a sign change. (b) The corresponding reflection phases $\varphi_{0,r}$ and the transmission $|t_{0,r}|^2$ of a $N = 20$ cell chain in the “A” ($\Phi = 0.48$) and “D” classes. (c) Same as (a), for the $\lambda = 1$ configuration, with the horizontal line marking the sign change. (d) $\varphi_{1,r}$ and $|t_{1,r}|^2$ for $\lambda = 1$. The scattering energy is $E = 0$, the Fermi level. The tunneling amplitudes are $j_3 = 0.2$, $J_c = 0.3$, and $J_0 = 2.0$ (units of j_2).

[Fig. 1(c)], and then

$$\mathcal{F}_\lambda(E) \begin{bmatrix} \Psi_a(1) \\ \Psi_\chi(N) \end{bmatrix} = J_c \begin{bmatrix} A_L + B_L \\ A_R + B_R \end{bmatrix}. \quad (6)$$

The matrix $\mathcal{F}_\lambda(E)$ is detailed in Ref. [25]. The eigenenergies of an isolated chain, $J_c = 0$, are given by $\det[\mathcal{F}_\lambda(E)] = 0$. Otherwise,

$$\mathcal{S}_\lambda \equiv \begin{bmatrix} r_{\lambda,l} & t_{\lambda,r} \\ t_{\lambda,l} & r_{\lambda,r} \end{bmatrix} = -1 - 2i \sin(\kappa) [e^{-i\kappa} - \Lambda \mathcal{F}_\lambda^{-1}]^{-1}, \quad (7)$$

$$\Lambda = (J_c^2/J_0),$$

where $r_{\lambda,l}$ ($r_{\lambda,r}$) and $t_{\lambda,l}$ ($t_{\lambda,r}$) are the reflection and transmission amplitudes from the left (right) in the λ configuration, and the unitarity of \mathcal{S}_λ is ensured by $\mathcal{F}_\lambda = \mathcal{F}_\lambda^\dagger$.

Size effects. In the $\lambda = 0$ configuration the reflection amplitudes at the Fermi energy ($E = 0$) are

$$r_{0,l/r} = -\frac{\Lambda^2 e^{(N-1)\alpha} \pm 2i\xi \Lambda S_{N-1} + |W| e^{-N\alpha}}{\Lambda^2 e^{(N-1)\alpha} - 2i\xi \Lambda S_{N-1} - |W| e^{-N\alpha}}, \quad (8)$$

where $\xi = 2j_1 j_2 j_3 \cos \Phi (j_1^2 - j_2^2)$, $S_n = \sinh[n\alpha]$, and $\exp[\alpha] = -|j_2/j_1|$ for $E = 0$. For the most symmetric classes “BDI” ($j_3 = 0$) and “D” ($\Phi = \pi/2$),

$$r_{0,l} = r_{0,r} = \left(\left| \frac{j_1}{j_2} \right|^{2N} - \frac{\Lambda^2}{j_2^2} \right) \left(\left| \frac{j_1}{j_2} \right|^{2N} + \frac{\Lambda^2}{j_2^2} \right)^{-1}. \quad (9)$$

The reflection amplitude is negative for $|j_1/j_2| < \gamma_N$ with $\gamma_N = |\Lambda/j_2|^{1/N}$ being the parameter indicating the finite-size effect, and is positive otherwise, see Fig. 2(a). At $|j_1/j_2| = \gamma_N$, the reflection amplitude changes from -1 to $+1$, and the transmission is peaked. This is distinct from the size effect on the threshold for the emergence of edge states in the isolated

SSH chain, $|j_1/j_2| < N/(N+1)$ [9], based on the Bloch spectrum. The size effect in an isolated chain is fully determined by the chain length N , reducing the range for the edge states, as compared to $|j_1/j_2| < 1$. Within the scattering formalism, the size effect is determined by both N and Λ . Importantly, for $|\Lambda/j_2| > 1$, i.e., for $\gamma_N > 1$, the range of negative reflection amplitudes can exceed that of the nontrivial phase. Then a negative reflection amplitude gives a false indication of the system topology. Nonetheless, there is a transmission peak, with $|j_1/j_2| = \gamma_N$, where the reflection passes through zero, as seen in Fig. 2(b). That peak coincides with the one found before [9] only for $N \rightarrow \infty$, where $\gamma_N = 1$. Such a peak has been proposed as a signal of TPT [4]. Its dependence on the coupling with the leads casts doubts on this identification.

For the “AI” and “A” classes, the reflection amplitudes $r_{0,l} \neq r_{0,r}$ in Eq. (8) are complex. The reflection phases $\varphi_{0,l} \equiv \arg[r_{0,l}]$ and $\varphi_{0,r} \equiv \arg[r_{0,r}]$ vary smoothly with $|j_1/j_2|$, and the amplitudes do not cross zero around $|j_1/j_2| = 1$, excluding the possibility of a transmission peak of unit magnitude. Interestingly, this peak still appears near the topological axes in Fig. 1(b), but decays away from these axes: It does not imply a TPT.

The size effect can be removed in the $\lambda = 1$ configuration, where at the Fermi energy

$$r_{1,l/r} = \frac{\xi \mp i\Lambda}{\xi + i\Lambda \coth[(N-1)\alpha]}. \quad (10)$$

Thus, $r_{1,l} = -r_{1,r} = -\tanh[(N-1)\alpha]$ for $\xi = 0$. Since $\exp[\alpha] = -|j_1/j_2|$ at $E = 0$, the left (right) reflection is negative (positive) for $|j_1/j_2| < 1$, changing the sign of $r_{1,l(r)}$ as required by the TPT’s criterion in the “BDI” or “D” class. However, the different signs of $r_{1,l(r)}$ may lead to conflicting predictions of the topology. For instance, $r_{1,l} = -1$ for $|j_1/j_2| < 1$ indicates a topological phase, but $r_{1,r} = 1$ corresponds to a trivial phase. This contradiction can be traced to the lack of a b site at the rightmost cell, making the chain an “incomplete” one, for which it is impossible to define PH and chiral symmetries, as opposed to the case of a two-sublattice chain of N unit cells (details in Ref. [25]). Thus, without preliminary knowledge of the ends’ configuration of a finite chain, a one-sided reflection does not fully determine the topology of a finite system. Peaks of the transmission are predicted in many cases, but their relation to the TPT’s of finite chains remains questionable.

Edge states in low-symmetry classes. The reflection amplitudes at $E = 0$ of the “AI” and “A” classes are complex [Eq. (10)], and cannot jump from -1 to $+1$ upon changing $|j_1/j_2|$ as for the “D” class. But examining the variations of the reflection phases in Figs. 3(a) and 3(b) shows that a negative reflection amplitude can appear at certain points in the j_1 - E plane for these classes, depending on the endpoints’ configuration [25]. Figures 3(c) and 3(d) confirm that there are edge states for which the reflection amplitudes are negative.

In general, the reflection amplitude is [25]

$$r_{\lambda,l/r} = -1 - \frac{2i(\det[\mathcal{F}_\lambda] e^{-i\kappa} - \Lambda \mathcal{F}_{\lambda,11/22}) \sin \kappa}{\det[\mathcal{F}_\lambda] e^{-2i\kappa} - \Lambda \text{Tr}[\mathcal{F}_\lambda] e^{-i\kappa} + \Lambda^2}. \quad (11)$$

When the scattering energy resonates with an eigenenergy of the isolated chain, i.e., for $\det[\mathcal{F}_\lambda(E)] = 0$, a negative

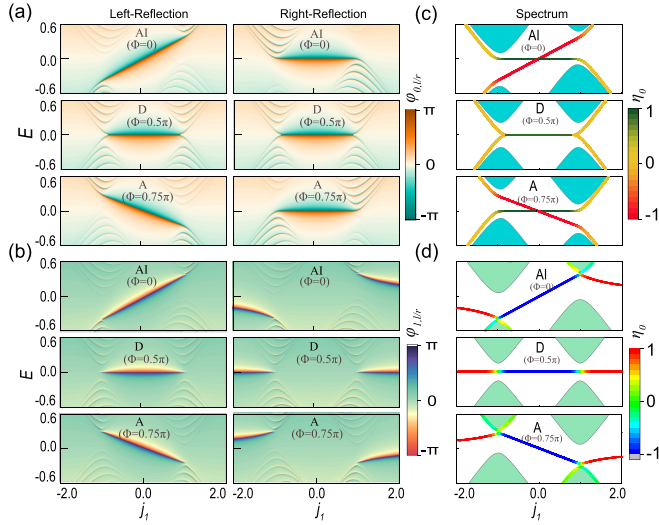


FIG. 3. Comparison of features of the “AI,” “D,” and “A” classes (for AB fluxes marked on the panels) in the $\lambda = 0$ [(a) and (c)] and $\lambda = 1$ [(b) and (d)] configurations. (a), (b) The phases’ distribution of the reflection amplitudes off the two endpoints in the j_1 - E plane. (c), (d) The energy spectra of isolated chains ($N = 20$) as functions of j_1 . The sidebar indicates the extent of the states formed in the gap (η_0 is defined in the text). Tunneling amplitudes as in Fig. 2.

reflection on the left/right endpoint appears only if $\mathcal{F}_{\lambda,11/22} = 0$. However, in a finite chain, the two conditions are not compatible: for $\mathcal{F}_{\lambda,mm} = 0$, $\det[\mathcal{F}_\lambda] = -\mathcal{F}_{\lambda,12}\mathcal{F}_{\lambda,21} \propto \exp[-2N\alpha]$ which differs from zero, unless E is located in the energy gap ($\exp[\alpha(E)] < -1$) and $N \rightarrow \infty$. Thus, a left/right edge state in the band gap of a sufficiently long isolated chain can coexist with a negative reflection amplitude from that side.

In the $\lambda = 0$ configuration, this situation is realized for

$$\begin{aligned} \mathcal{F}_{0,22} &= 0 \quad \forall \{E = 0, \quad j_2^2 > j_1^2\}, \\ \mathcal{F}_{0,11} &= 0 \quad \forall \{E = \varepsilon_2, \quad \varepsilon_2^2 + j_2^2 > j_1^2\}, \end{aligned} \quad (12)$$

where $\varepsilon_2 \equiv \xi(j_1^2 - j_2^2)/(j_2^2 + j_3^2)$. The vanishing of $\mathcal{F}_{0,22}$ implies the appearance of a negative reflection amplitude on the right side [see Fig. 3(a)], corresponding to a (right) edge state around $E = 0$ as shown in Fig. 3(c). The extent of the edge states is quantified by $\eta_0 \equiv \sum_{i=1}^5 |V_i|^2 - \sum_{i=N-4}^N |V_i|^2$, with the left (right) edge state characterized by $\eta_0 \sim 1$ (-1). The energy ε_2 at which $\mathcal{F}_{0,11}$ vanishes varies with Φ [25]. As it increases, it “pushes” the system from the “AI” class to the “A” one, passing through “D,” broadening the parameter range available for ε_2 compared to that for the right endpoint.

The persistent appearance of a zero-energy edge state at the rightmost side of the chain in all four classes [see Fig. 3(c)] is due to the protection of the subchiral symmetry possessed by the b sites [30–32]. The chiral symmetry of the two-sublattice chain is broken once $j_3 \neq 0$ (leading to a - a tunneling), rendering the energy of the edge state located at the left side to differ from zero, while the b sublattice still maintains the chiral symmetry [31].

For the $\lambda = 1$ configuration, a right-side edge state appears when

$$\mathcal{F}_{1,22} = 0 \quad \forall \{E = \varepsilon_1, \quad \varepsilon_1^2 + j_1^2 > j_2^2\}, \quad (13)$$

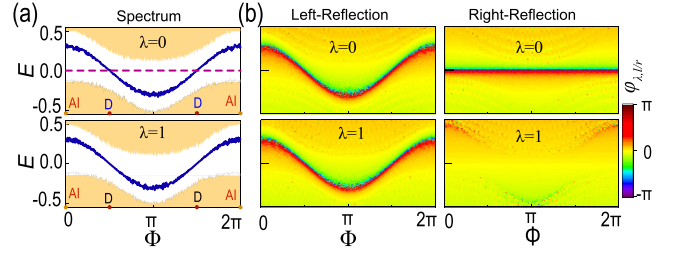


FIG. 4. (a) Energy spectra of a finite disordered isolated chain (parameters as in Fig. 2) as functions of Φ in the $\lambda = 0, 1$ configurations with $j_1 = 0.8j_2$. The left and right edge states are indicated by the solid and dashed lines. (b) The phases of the reflection amplitudes of the disordered chain in the Φ - E plane. The disorder is modeled by adding to the tunneling amplitude j_1 a random term, $\delta j_{1,n} = 0.3(w_n - 0.5)$, with $w_n \in [0, 1]$ being a random number.

where $\varepsilon_1 \equiv \xi(j_1^2 - j_2^2)/(j_1^2 + j_3^2)$. Interestingly, for $\xi = 0$ the right-side edge state appears for $|j_2/j_1| < 1$, the opposite range to that of the left side, $|j_2/j_1| > 1$ [see Eq. (12)]. It follows that there is always a zero-energy state in the band gap, as seen in Fig. 3(d). This results from the fact that for $\lambda = 1$, the chain comprises two two-sublattice subchains, connected at kink (see Fig. S4 in Ref. [25]). The left subchain is isomorphic to a finite chain in the $\lambda = 0$ configuration. Interchanging the roles of j_1 and j_2 in the right subchain shows that the two have mirror symmetry with respect to the kink. This swapping of j_1 and j_2 explains the parameter ranges found above.

Scattering theory is also useful for probing the edge states of a disordered chain belonging to a low-symmetry class. Figure 4(a) portrays the energy spectra of an isolated disordered chain coupled to leads in the two configurations $\lambda = 0, 1$. As seen, with the change of the AB flux, the energy of the edge states is robust (“protected”) against a weak disorder. As the symmetry class is varied, “AI” \rightarrow “A” \rightarrow “D” $\rightarrow \dots \rightarrow$ “AI,” there appear two edge states for $\lambda = 0$: A zero-energy edge state located at the right side and a nonzero-energy one at the opposite side. For $\lambda = 1$, j_1 and j_2 are not in the range securing $\mathcal{F}_{1,22} = 0$ [see Eq. (13)], and thus the zero-energy (right) edge state disappears. The trend of variation of the left and right edge states is reflected in the conditions required for negative reflection amplitudes, see Fig. 4(b).

Conclusions. By studying the scattering properties of a finite triangle chain coupled to two semiinfinite leads, we could follow the conditions for the appearance of edge states and their relationships with the reflection amplitudes’ phases in several symmetry classes, topological as well as nontopological. In particular, we show that a negative reflection amplitude can appear in nontopological classes, and can be correlated with the appearance of edge states, even in the presence of weak disorder, rendering these features as dubious indicators of a topological transition. Our study compares in detail the reflection amplitudes and edge states on both endpoints of a finite system, emphasizing the dependence on the length of the chain and the configuration of its coupling to the leads. Since scattering properties can be measured on finite chains (say, of cold atoms) at low temperatures, and as we have found that (i) weak disorder is not detrimental for edge states and (ii) by applying Aharonov-Bohm flux the system can “flow”

in the space of symmetry classes, it is hoped that our study will invoke more interest regarding the characterization of topological materials via scattering properties.

Acknowledgment. This work is supported by the National Natural Science Foundation of China (Grants No. 92165208 and No. 11874071).

-
- [1] M. Z. Hasan and C. L. Kane, *Colloquium: Topological insulators*, *Rev. Mod. Phys.* **82**, 3045 (2010).
- [2] X.-L. Qi and S.-C. Zhang, Topological insulators and superconductors, *Rev. Mod. Phys.* **83**, 1057 (2011).
- [3] A. Bansil, H. Lin, and T. Das, *Colloquium: Topological band theory*, *Rev. Mod. Phys.* **88**, 021004 (2016).
- [4] I. C. Fulga, F. Hassler, A. R. Akhmerov, and C. W. J. Beenakker, Scattering formula for the topological quantum number of a disordered multimode wire, *Phys. Rev. B* **85**, 155429 (2011).
- [5] I. C. Fulga, F. Hassler, and A. R. Akhmerov, Scattering theory of topological insulators and superconductors, *Phys. Rev. B* **85**, 165409 (2012).
- [6] B. Sbierski and P. W. Brouwer, Z_2 phase diagram of three-dimensional disordered topological insulators via a scattering matrix approach, *Phys. Rev. B* **89**, 155311 (2014).
- [7] A. Bissonnette, N. Delnour, A. Mckenna, H. Eleuch, M. Hilke, and R. MacKenzie, Boundary-induced topological transition in an open Su-Schrieffer-Heeger model, *Phys. Rev. B* **109**, 075106 (2024).
- [8] C. Mahaux and H. A. Weidenmüller, Comparison between the R-matrix and eigenchannel methods, *Phys. Rev.* **170**, 847 (1968).
- [9] P. Delplace, D. Ullmo, and G. Montambaux, Zak phase and the existence of edge states in graphene, *Phys. Rev. B* **84**, 195452 (2011).
- [10] M. Atala, M. Aidelsburger, J. T. Barreiro, D. Abanin, T. Kitagawa, E. Demler, and I. Bloch, Direct measurement of the Zak phase in topological Bloch bands, *Nat. Phys.* **9**, 795 (2013).
- [11] W. P. Su, J. R. Schrieffer, and A. J. Heeger, Solitons in polyacetylene, *Phys. Rev. Lett.* **42**, 1698 (1979).
- [12] A. Altland and M. R. Zirnbauer, Nonstandard symmetry classes in mesoscopic normal-superconducting hybrid structures, *Phys. Rev. B* **55**, 1142 (1997).
- [13] S. Ryu, A. P. Schnyder, A. Furusaki, and A. W. W. Ludwig, Topological insulators and superconductors: tenfold way and dimensional hierarchy, *New J. Phys.* **12**, 065010 (2010).
- [14] G. Cáceres-Aravena, B. Real, D. Guzmán-Silva, A. Amo, L. E. F. Foa Torres, and R. A. Vicencio, Experimental observation of edge states in SSH-Stub photonic lattices, *Phys. Rev. Res.* **4**, 013185 (2022).
- [15] S. K. Kanungo, J. D. Whalen, Y. Lu, M. Yuan, S. Dasgupta, F. B. Dunning, K. R. A. Hazzard, and T. C. Killian, Realizing topological edge states with Rydberg-atom synthetic dimensions, *Nat. Commun.* **13**, 972 (2022).
- [16] S. Mukherjee, M. D. Liberto, P. Öhberg, R. R. Thomson, and N. Goldman, Experimental observation of aharonov-bohm cages in photonic lattices, *Phys. Rev. Lett.* **121**, 075502 (2018).
- [17] M. Kremer, I. Petrides, E. Meyer, M. Heinrich, O. Zilberberg, and A. Szameit, A square-root topological insulator with non-quantized indices realized with photonic Aharonov-Bohm cages, *Nat. Commun.* **11**, 907 (2020).
- [18] W. Gou, T. Chen, D. Xie, T. Xiao, T.-S. Deng, B. Gadway, W. Yi, and B. Ya, Tunable nonreciprocal quantum transport through a dissipative aharonov-bohm ring in ultracold atoms, *Phys. Rev. Lett.* **124**, 070402 (2020).
- [19] H. Li, Z. Dong, S. Longhi, Q. Liang, D. Xie, and B. Yan, Aharonov-bohm caging and inverse anderson transition in ultracold atoms, *Phys. Rev. Lett.* **129**, 220403 (2022).
- [20] G. Harari, M. A. Bandres, Y. Lumer, M. C. Rechtsman, Y. D. Chong, M. Khajavikhan, D. N. Christodoulides, and M. Segev, Topological insulator laser: Theory, *Science* **359**, eaar4003 (2018).
- [21] The energy spectra of a two-dimensional lattice that can belong to several classes upon varying bonding features have been recently analyzed, see A. Agrawal and J. N. Bandyopadhyay, Cataloging topological phases of N stacked Su-Schrieffer-Heeger chains by a systematic breaking of symmetries, *Phys. Rev. B* **108**, 104101 (2023).
- [22] P. St-Jean, V. Goblot, E. Galopin, A. Lemaître, T. Ozawa, L. Le Gratiet, I. Sagnes, J. Bloch, and A. Amo, Lasing in topological edge states of a 1D lattice, *Nat. Photon.* **11**, 651 (2017).
- [23] B. Ostahie and A. Aldea, Spectral analysis, chiral disorder and topological edge states manifestation in open non-Hermitian Su-Schrieffer-Heeger chains, *Phys. Lett. A* **387**, 127030 (2021).
- [24] S. Garmon and K. Noba, Reservoir-assisted symmetry breaking and coalesced zero-energy modes in an open PT-symmetric Su-Schrieffer-Heeger model, *Phys. Rev. A* **104**, 062215 (2021).
- [25] See Supplemental Material at <http://link.aps.org/supplemental/10.1103/PhysRevB.109.L081408> for details of the symmetry classification of the triangle chain using the Bloch band theory and Zak phases, as well as derivations of the transfer \mathcal{T} and scattering S_λ matrices for the various configurations, which also includes Refs. [26–28].
- [26] C.-K. Chiu, J. C. Y. Teo, A. P. Schnyder, and S. Ryu, Classification of topological quantum matter with symmetries, *Rev. Mod. Phys.* **88**, 035005 (2016).
- [27] M. Ezawa, Y. Tanaka, and N. Nagaosa, Topological phase transition without gap closing, *Sci. Rep.* **3**, 2790 (2013).
- [28] L. Li, C. Yang, and S. Chen, Winding numbers of phase transition points for one-dimensional topological systems, *Europhys. Lett.* **112**, 10004 (2015).
- [29] J. Zak, Berry's phase for energy bands in solids, *Phys. Rev. Lett.* **62**, 2747 (1989).
- [30] M. Jangjan and M. V. Hosseini, Topological properties of subsystem-symmetry-protected edge states in an extended quasi-one-dimensional dimerized lattice, *Phys. Rev. B* **106**, 205111 (2022).
- [31] Z. Wang, X. Wang, Z. Hu, D. Bongiovanni, D. Jukić, L. Tang, D. Song, R. Morandotti, Z. Chen, and H. Buljan, Sub-symmetry-protected topological states, *Nat. Phys.* **19**, 992 (2023).
- [32] F. Liu, Analytic solution of the n -dimensional Su-Schrieffer-Heeger model, *Phys. Rev. B* **108**, 245140 (2023).